HDL and Glut1 inhibition reverse a hypermetabolic state in mouse models of myeloproliferative disorders

Emmanuel L. Gautier,[1] Marit Westerterp,[2,3] Neha Bhagwat,[4,5] Serge Cremers,[2] Alan Shih,[4,5] Omar Abdel-Wahab,[4,5] Dieter Lütjohann,[6] Gwendalyn J. Randolph,[1] Ross L. Levine,[4,5] Alan R. Tall,[2] and Laurent Yvan-Charvet[2,7]

[1]Department of Pathology and Immunology, Washington University in St. Louis School of Medicine, St. Louis, MO 63110
[2]Department of Medicine, Division of Molecular Medicine, Columbia University, New York, NY 10032
[3]Department of Medical Biochemistry, Academic Medical Center of Amsterdam, University of Amsterdam, 1105 Amsterdam, Netherlands
[4]Human Oncology and Pathogenesis Program; and [5]Leukemia Service, Department of Medicine; Memorial Sloan-Kettering Cancer Center, New York, NY 10065
[6]Institute of Clinical Chemistry and Clinical Pharmacology, University Clinic Bonn, 53127 Bonn, Germany
[7]Institut National de la Santé et de la Recherche Médicale U1065, Centre Mediterraneen de Medecine Moleculaire (C3M), Avenir, 06204 Nice, France

A high metabolic rate in myeloproliferative disorders is a common complication of neoplasms, but the underlying mechanisms are incompletely understood. Using three different mouse models of myeloproliferative disorders, including mice with defective cholesterol efflux pathways and two models based on expression of human leukemia disease alleles, we uncovered a mechanism by which proliferating and inflammatory myeloid cells take up and oxidize glucose during the feeding period, contributing to energy dissipation and subsequent loss of adipose mass. In vivo, lentiviral inhibition of Glut1 by shRNA prevented myeloproliferation and adipose tissue loss in mice with defective cholesterol efflux pathway in leukocytes. Thus, Glut1 was necessary to sustain proliferation and potentially divert glucose from fat storage. We also showed that overexpression of the human ApoA-I transgene to raise high-density lipoprotein (HDL) levels decreased Glut1 expression, dampened myeloproliferation, and prevented fat loss. These experiments suggest that inhibition of Glut-1 and HDL cholesterol–raising therapies could provide novel therapeutic approaches to treat the energy imbalance observed in myeloproliferative disorders.

CORRESPONDENCE
Laurent Yvan-Charvet:
ly2159@columbia.edu

Abbreviations used: 2-[^{14}C]-DG, 2-[^{14}C]-deoxyglucose; 2-NBDG, 2-[*N*-(7-nitrobenz-2-oxa-1, 3-diazol-4-yl)amino]-2-deoxy-D-glucose; ACL, ATP-citrate lyase; HDL, high-density lipoprotein; HSC, hematopoietic stem cell; PDP, pyruvate dehydrogenase phosphoserine phosphatase; PFK, phosphofructokinase; RQ, respiratory quotient; SDH, succinate dehydrogenase; TCA, tricarboxylic acid; TMRE, tetramethylrhodamine ethyl ester.

Chronic inflammatory diseases such as chronic infection, cancer, and heart failure are often associated with adipose tissue loss (Delano and Moldawer, 2006). Adipose tissue loss in the setting of chronic inflammatory diseases could ultimately represent a major health problem because of associated comorbidities such as weakness, fatigue, and impaired immunity. Loss of adipose tissue is ultimately caused by an imbalance between food intake and energy expenditure. Although food intake is often reduced in patients with chronic inflammatory diseases, these patients exhibit a persistent state of inappropriately high metabolic rate, and this substantially contributes to their adipose loss (Delano and Moldawer, 2006). However, the link between chronic inflammation, tissue metabolism, and enhanced energy expenditure in this state of chronic hypermetabolism is not fully understood.

Among chronic inflammatory diseases, hematological malignancies such as leukemias and myeloproliferative disorders are also associated with adipose tissue loss (Dingli et al., 2004). In humans, among the most common activating mutations in myeloid malignancies are mutations in the *FMS-like tyrosine kinase 3* (*Flt3*) gene, which occur in ∼30% of cases of acute myeloid leukemia as well as mutations in the

The Rockefeller University Press $30.00
J. Exp. Med. 2013 Vol. 210 No. 2 339-353
www.jem.org/cgi/doi/10.1084/jem.20121357

The Journal of Experimental Medicine

thrombopoietin receptor (proto-oncogene c-Mpl) observed in 5–10% of patients with myelofibrosis. These mutations confer a fully penetrant myeloproliferative disorder in mice (Kelly et al., 2002; Pikman et al., 2006), providing a useful tool for studying the mechanism of adipose tissue loss associated with myeloproliferative disorders.

We have recently shown that mice lacking the cholesterol efflux transporters ABCA1 and ABCG1 develop massive expansion and proliferation of hematopoietic stem and progenitor cells, marked monocytosis, neutrophilia, and infiltration of various organs with myeloid cells, resembling a classical myeloproliferative disorder (Hansson and Björkholm, 2010; Yvan-Charvet et al., 2010). As we noticed a dramatic loss of adipose tissue in *Abca1*$^{-/-}$*Abcg1*$^{-/-}$ BM chimeras, we hypothesized that the myeloproliferative disorder of these mice might be responsible for their wasting syndrome and proceeded to investigate the underlying mechanisms.

RESULTS

Lack of ABCA1 and ABCG1 in hematopoietic cells promotes adipose tissue atrophy

Determination of the fat and muscle mass of irradiated WT recipients transplanted with *Abca1*$^{-/-}$*Abcg1*$^{-/-}$ BM cells fed a chow diet revealed not only absence of adipose tissue growth but also reduced epididymal fat mass at 24 wk after reconstitution compared with controls (Fig. 1 A). Gastrocnemius muscle loss was also observed 30 wk after reconstitution in these mice (Fig. 1 B). Subcutaneous and retroperitoneal adipose depots were also decreased by more than threefold at 24 wk after reconstitution in *Abca1*$^{-/-}$*Abcg1*$^{-/-}$ BM chimeras, consistent with their reduced plasma leptin levels (Table 1). To test whether the adipose tissue atrophy of these mice was a direct consequence of their defective hematopoietic compartment and myeloproliferative syndrome (Yvan-Charvet et al., 2010), we generated hematopoietic stem cell (HSC)–specific chimeric animals by transplanting lethally irradiated WT recipients with purified WT or *Abca1*$^{-/-}$*Abcg1*$^{-/-}$ HSCs (Lin^{-}Sca^{+}cKit^{+}, LSK fraction). Mice transplanted with *Abca1*$^{-/-}$*Abcg1*$^{-/-}$ LSK cells reproduced the threefold increase in the Gr-1^{hi}/CD11b^{hi} blood myeloid population observed in *Abca1*$^{-/-}$*Abcg1*$^{-/-}$ BM transplanted mice (Yvan-Charvet et al., 2010) and exhibited a twofold reduction in fat mass 12 wk after reconstitution (Fig. 1 A). Similar findings were observed in mice with specific knockout of these transporters in the hematopoietic lineage (Mx1-Cre Abca1$^{fl/fl}$Abcg1$^{fl/fl}$) 10 wk after injections of PolyI:C to excise the STOP codon that prevents the expression of the cre recombinase (Fig. 1 C). Together, these observations revealed that the expansion of adipose tissue is severely compromised in mice lacking ABCA1 and ABCG1 in their hematopoietic system.

ABCA1 and ABCG1 deficiency in leukocytes impacts glucose homeostasis

We next compared the metabolic characteristics of chow-fed *Abca1*$^{-/-}$*Abcg1*$^{-/-}$ BM transplanted mice and their respective controls by indirect calorimetry. No significant changes in daily food intake, energy expenditure, or locomotor activity were observed in these mice (Table 1). Similar fat and cholesterol absorption and bile acid excretion were also observed in *Abca1*$^{-/-}$*Abcg1*$^{-/-}$ mice (not depicted). However, *Abca1*$^{-/-}$*Abcg1*$^{-/-}$ BM transplanted mice exhibited a higher respiratory quotient (RQ) during the feeding period (dark phase; Fig. 1 D), reflecting an ∼20% increase in glucose oxidation (Fig. 1 E) and exhibited hypoglycemia (Table 1). Injection i.p. of a glucose bolus also revealed faster glucose utilization in *Abca1*$^{-/-}$*Abcg1*$^{-/-}$ BM transplanted mice compared with WT transplanted controls (Fig. 1 F). We next examined the uptake of the radiolabeled D-glucose analogue 2-[^{14}C]-deoxyglucose (2-[^{14}C]-DG) in *Abca1*$^{-/-}$*Abcg1*$^{-/-}$ BM transplanted mice in the fed state. No significant changes were observed in the total uptake of 2-[^{14}C]-DG in the skeletal muscle and brain (Fig. 1 G), whereas, in line with their reduced fat mass, total 2-[^{14}C]-DG incorporation was reduced in their adipose tissue (Fig. 1 G). In contrast, the total uptake of 2-[^{14}C]-DG was increased by two- to threefold in the heart, lung, spleen, and BM of these mice (Fig. 1 G) and by ∼1.5-fold when expressed as the rate constant for net tissue uptake of 2-[^{14}C]-DG uptake (Fig. 1 H). Thus, we showed that *Abca1*$^{-/-}$*Abcg1*$^{-/-}$ BM transplanted mice have increased propensity to clear and use glucose.

Inflammation diverts glucose from fat storage by promoting adipose tissue insulin resistance in *Abca1*$^{-/-}$*Abcg1*$^{-/-}$ BM transplanted mice

Consistent with their myeloproliferative disorder, *Abca1*$^{-/-}$*Abcg1*$^{-/-}$ BM chimeras exhibited a chronic inflammatory state as reflected by a threefold increase in plasma TNF levels (Table 1). Microscopic examination of the adipose tissue of *Abca1*$^{-/-}$*Abcg1*$^{-/-}$ BM transplanted mice revealed an increased inflammatory infiltrate reflected by crown-like structures (Fig. 2 A). Because infiltrated leukocytes are a hallmark of insulin resistance in adipose tissue (Lumeng and Saltiel, 2011; Odegaard and Chawla, 2011), we wondered whether the adipose tissue infiltration observed in *Abca1*$^{-/-}$*Abcg1*$^{-/-}$ BM chimeras would promote local insulin resistance and contribute to their reduced adipose tissue glucose uptake. To address this question, a bolus of insulin was injected into WT and *Abca1*$^{-/-}$*Abcg1*$^{-/-}$ BM transplanted mice, and hallmarks of insulin signaling (AKT phosphorylation and GLUT4 addressing to the cell membrane) were assessed. Western blot analysis revealed reduced GLUT4 translocation from the low-density microsome fraction to the plasma membrane in response to insulin in the adipose tissue of *Abca1*$^{-/-}$*Abcg1*$^{-/-}$ BM transplanted mice (Fig. 2 B). This was associated with reduced AKT phosphorylation, suggesting insulin resistance in adipocytes is secondary to local inflammatory cell infiltration (Fig. 2 B). Accordingly, microscopic analysis of isolated adipocytes revealed smaller adipocytes in WT recipients transplanted with *Abca1*$^{-/-}$*Abcg1*$^{-/-}$ BM cells (Fig. 2 A and Table 1), whereas adipocyte cell numbers were comparable with controls (Table 1). Finally, depletion of Ly6C/G^{+}

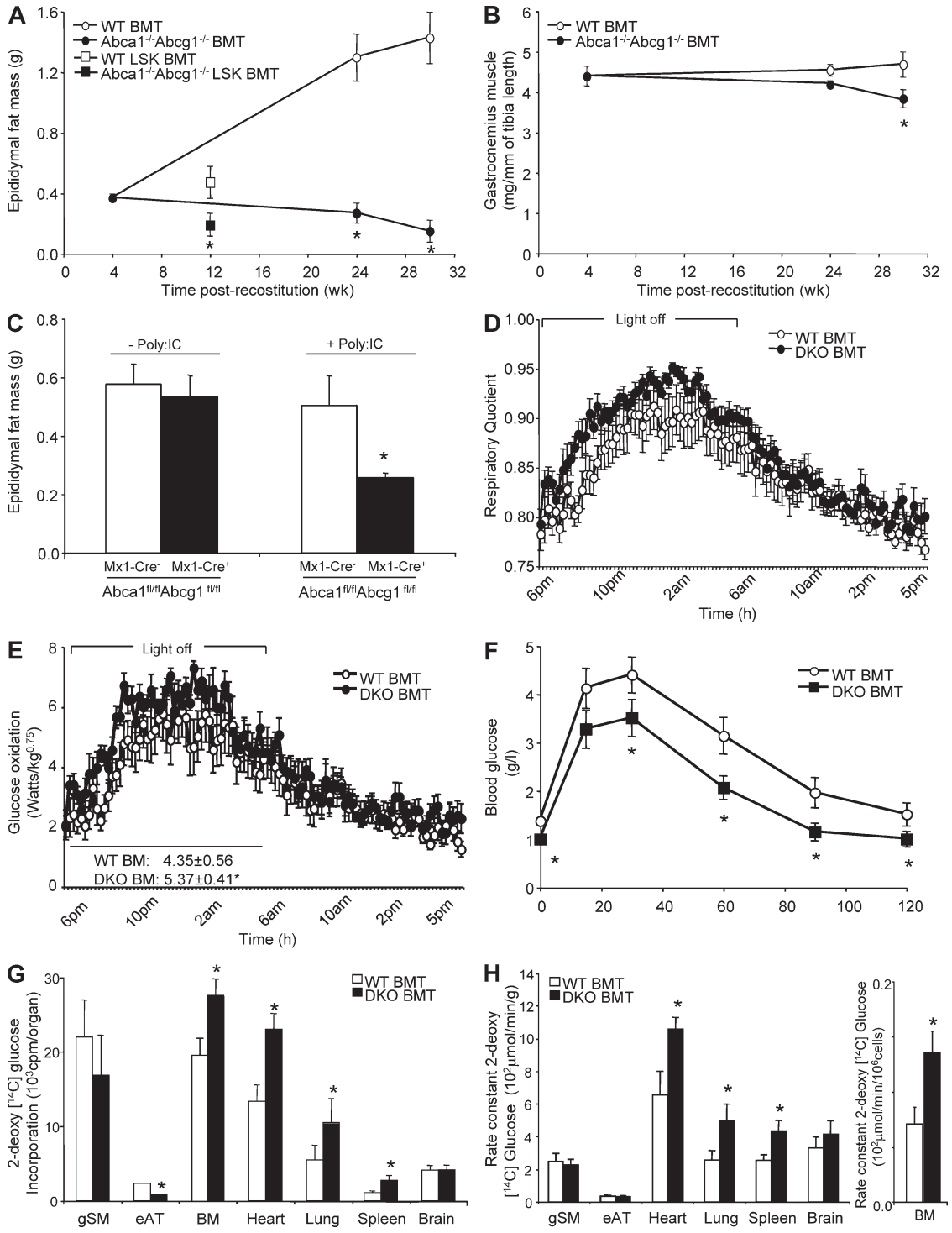

Figure 1. Adipose tissue atrophy and enhanced glucose utilization in *Abca1*$^{-/-}$*Abcg1*$^{-/-}$ BM chimeras. (A) Epididymal adipose tissue of WT recipient mice transplanted with WT or *Abca1*$^{-/-}$*Abcg1*$^{-/-}$ BM cells or WT and *Abca1*$^{-/-}$*Abcg1*$^{-/-}$ HSC (Lin^{-}Sca^{+}cKit^{+}, LSK fraction) transplanted mice. (B) Gastrocnemius skeletal muscle mass of these mice. (C) Epididymal fat mass in mice with specific knockout of these transporters in the hematopoietic lineage (Mx1-Cre Abca1$^{fl/fl}$Abcg1$^{fl/fl}$) 10 wk after three injections of 15 mg/kg PolyI:C to excise the STOP codon. (D and E) RQ (D) and glucose oxidation efficiency (E) measured by indirect calorimetry in chow-fed WT and *Abca1*$^{-/-}$*Abcg1*$^{-/-}$ BM transplanted (BMT) mice 10 wk after reconstitution. (F) Glucose tolerance test was performed i.p. on chow-fed WT and *Abca1*$^{-/-}$*Abcg1*$^{-/-}$ BM transplanted mice 12 wk after reconstitution. Blood glucose concentrations were measured at the indicate time points. (G and H) Tissue uptake (G) and rate constant of 2-[^{14}C]-DG (H) in 24-wk-old chow-fed WT and *Abca1*$^{-/-}$*Abcg1*$^{-/-}$ BM transplanted mice at the end of the study period (40 min after i.v. injection of the radiolabeled tracer). All results are means ± SEM and are representative of an experiment of five to seven animals per group. *, $P < 0.05$ versus WT.

Table 1. Effect of leukocyte ABCA1 and ABCG1 deficiencies on body weight, plasma leptin levels, subcutaneous and retroperitoneal adipose depots, plasma glucose, insulin and TNF levels, epididymal adipose tissue cellularity, and energy metabolism

Metabolic parameters	BM transplantation	
	WT	*Abca1*$^{-/-}$*Abcg1*$^{-/-}$
Body weight (g)	27.9 ± 0.9	27.4 ± 0.6
Plasma Leptin (ng/ml)	1.95 ± 0.4	0.7 ± 0.2*
Subcutaneous fat mass (g)	0.52 ± 0.12	0.15 ± 0.03*
Retroperitoneal fat mass (g)	0.28 ± 0.04*	0.09 ± 0.08*
Plasma glucose (g/liter)	2.1 ± 0.1	1.7 ± 0.1*
Plasma Insulin (ng/ml)	7.9 ± 0.8	6.1 ± 1.1
Plasma TNF (pg/ml)	3.1 ± 0.5	7.4 ± 0.6*
Fat cell number (×10^6)	4.8 ± 0.9	4.6 ± 0.8
Fat cell weight (ng)	119 ± 14*	36 ± 5*
Food intake (g/day)	3.28 ± 0.14	3.33 ± 0.13
Food intake (g/day/$g^{0.75}$)	0.29 ± 0.01	0.29 ± 0.01
Energy expenditure, EE (W/$kg^{0.75}$)	6.68 ± 0.25	7.11 ± 0.18
Locomotor activity (counts/14 min)	2,589 ± 544	2,560 ± 499

Values are mean ± SEM (n = 5 per group). *, P < 0.05 versus controls.

myeloid cells with the anti–granulocyte receptor-1 (Gr-1) antibody RB6-8C5 partially reversed the reduced glucose uptake in the adipose tissue of *Abca1*$^{-/-}$*Abcg1*$^{-/-}$ mice (not depicted). Together, these results indicate that myeloproliferation and associated adipose tissue infiltration compromise adipose tissue function and likely contribute to the loss of fat in *Abca1*$^{-/-}$*Abcg1*$^{-/-}$ BM transplanted mice. Moreover, these findings revealed that *Abca1*$^{-/-}$*Abcg1*$^{-/-}$ BM chimeras can efficiently clear glucose despite being insulin resistant.

Glucose consumption by proliferating myeloid cells contributes to whole body glucose dissipation in *Abca1*$^{-/-}$*Abcg1*$^{-/-}$ BM transplanted mice

Although local inflammation promoted adipose tissue insulin resistance, this could not explain the enhanced glucose uptake by noninsulin-sensitive tissues (Fig. 1 G) contributing to enhanced whole body glucose oxidation during the feeding period (Fig. 1 E). Because these tissues exhibit massive myeloid infiltration in *Abca1*$^{-/-}$*Abcg1*$^{-/-}$ BM transplanted mice (Yvan-Charvet et al., 2007; Out et al., 2008), we next investigated the uptake of glucose by *Abca1*$^{-/-}$*Abcg1*$^{-/-}$ leukocytes. To estimate glucose utilization by flow cytometry, we used the fluorescent D-glucose analogue 2-[*N*-(7-nitrobenz-2-oxa-1,3-diazol-4-yl)amino]-2-deoxy-D-glucose (2-NBDG) as a tool that reflects the glucose bound to the cells and its uptake. Leukocytes isolated from *Abca1*$^{-/-}$*Abcg1*$^{-/-}$ BM revealed a significant 30% increase in 2-NBDG staining (Fig. 3 A). This increase was massive in monocytes and neutrophils when the increased cell number was taken into account (Fig. 3 B; Yvan-Charvet et al., 2010), accounting for the total uptake of 2-[^{14}C]-DG in the BM (Fig. 1 G). As glucose uptake depends on the glucose transporter (Glut) family (Herman and Kahn, 2006), we next assessed the mRNA expression levels of several members of this family, namely Glut1, Glut2, Glut3, Glut4, and Glut6. *Abca1*$^{-/-}$*Abcg1*$^{-/-}$ BM cells exhibited a twofold up-regulation of the glucose transporter Glut1 mRNA expression, which was also the most highly expressed Glut member in leukocytes (Fig. 3 C). Flow cytometry analysis showed a 30% increase in the cell surface expression of Glut1 in vivo in *Abca1*$^{-/-}$*Abcg1*$^{-/-}$ CD45$^+$ leukocytes (not depicted), including monocytes, neutrophils, and lymphocytes (Fig. 3 D), and this correlated with increased mitochondrial membrane potential (Fig. 3 E). Together, these findings show that leukocytes have a major role in glucose uptake in *Abca1*$^{-/-}$*Abcg1*$^{-/-}$ BM transplanted mice exhibiting a myeloproliferative syndrome. This resulted in enhanced whole body glucose oxidation that could explain the increased energy dissipation in these mice.

Signaling via the IL-3/GM-CSF receptor common β-subunit enhances the expression of Glut1 and glycolytic enzymes in proliferating *Abca1*$^{-/-}$*Abcg1*$^{-/-}$ leukocytes

We next set out to better understand the mechanism leading to increased glucose uptake in *Abca1*$^{-/-}$*Abcg1*$^{-/-}$ leukocytes. Up-regulation of Glut-1 by oncogenes such as Ras or Src has been reported (Flier et al., 1987), and we recently showed enhanced Ras-Erk signaling in *Abca1*$^{-/-}$*Abcg1*$^{-/-}$ BM cells at basal state and in response to the hematopoietic growth factors IL-3 and GM-CSF (Yvan-Charvet et al., 2010). Therefore, we investigated the expression of Glut1 in response to IL-3 in BM leukocytes. As shown in Fig. 3 F, Glut1 mRNA levels were increased upon stimulation with IL-3 in WT BM cells and were further increased in *Abca1*$^{-/-}$*Abcg1*$^{-/-}$ cells. Inhibition of the Ras signaling pathway using a farnesyl transferase inhibitor, known to prevent the anchorage of Ras

in the plasma membrane and to inhibit the proliferation of *Abca1*$^{-/-}$*Abcg1*$^{-/-}$ BM cells (Yvan-Charvet et al., 2010), normalized Glut1 mRNA expression to WT levels (Fig. 3 F). Further characterization of signaling pathways downstream of the IL-3/GM-CSF receptor common β-chain (Chang et al., 2003) showed that the phosphoinositide 3-kinase inhibitor LY294002 prevented IL-3–induced Glut1 mRNA expression in *Abca1*$^{-/-}$*Abcg1*$^{-/-}$ leukocytes (Fig. 3 F), similar to the effect of this inhibitor on the proliferation of these cells (Yvan-Charvet et al., 2010). Analysis of the rates of [^{14}C]glucose oxidation revealed that in basal and IL-3–stimulated conditions, *Abca1*$^{-/-}$*Abcg1*$^{-/-}$ leukocytes exhibited a higher glycolytic rate (Fig. 3 G). This effect was inhibited by removal of membrane cholesterol by cyclodextrin (Fig. 3 G), consistent with the cholesterol-dependent regulation of IL-3Rβ signaling (Yvan-Charvet et al., 2010). Analysis of genes of the glycolytic and lipid synthetic pathways also revealed up-regulation of hexokinase 2 (Hk2), phosphofructokinase (PFK), and ATP-citrate lyase (ACL) mRNAs in *Abca1*$^{-/-}$*Abcg1*$^{-/-}$ leukocytes that was dependent on the IL-3/GM-CSF receptor common β-chain signaling pathway (Fig. 3 H). Fumarase and succinate dehydrogenase (SDH) mRNA expression was also increased in response to IL-3 in *Abca1*$^{-/-}$*Abcg1*$^{-/-}$ leukocytes (Fig. 3 H). Together, our results point to the IL-3/GM-CSF receptor common β-chain/GLUT1 axis as a major determinant of the increased glucose uptake observed in *Abca1*$^{-/-}$*Abcg1*$^{-/-}$ leukocytes.

Metabolic profiling reveals increased glycolysis and oxidative phosphorylation in proliferating *Abca1*$^{-/-}$*Abcg1*$^{-/-}$ leukocytes

Further quantification of glycolytic metabolites by LC-MS showed higher glucose 6-phosphate/fructose 6-phosphate (G6P+F6P) and fructose 1,6-diphosphate (F1,6BP) levels in basal and IL-3–stimulated *Abca1*$^{-/-}$*Abcg1*$^{-/-}$ leukocytes (Fig. 4 A). Increased citric acid cycle metabolites (citrate, isocitrate, succinate, fumarate, and malate) and related mitochondrial products (GTP and FAD) were also observed in *Abca1*$^{-/-}$*Abcg1*$^{-/-}$ leukocytes under basal and/or IL-3–stimulated conditions (Fig. 4, B and C). Consistent with these findings, a higher ATP to ADP ratio was observed in proliferating *Abca1*$^{-/-}$*Abcg1*$^{-/-}$ leukocytes (Fig. 4 D). This was associated with increased mitochondrial membrane potential measured using a fluorescent tetramethylrhodamine ethyl ester (TMRE) dye (not depicted) and increased SDH activity in *Abca1*$^{-/-}$*Abcg1*$^{-/-}$ leukocytes (Fig. 4 E).

The increased glycolysis in *Abca1*$^{-/-}$*Abcg1*$^{-/-}$ leukocytes is required for proliferation

To test whether high levels of glycolysis are required for *Abca1*$^{-/-}$*Abcg1*$^{-/-}$ leukocyte proliferation, we next cultured cells with media containing galactose or glucose. Galactose enters glycolysis through the Leloir pathway, which occurs at a significantly lower rate than glucose entry into glycolysis (Bustamante and Pedersen, 1977). Fig. 4 F shows that under glucose-free DMEM (DMEM poor), addition of glucose but not galactose enhanced the proliferation of *Abca1*$^{-/-}$*Abcg1*$^{-/-}$ leukocytes to the level of high-glucose DMEM (DMEM rich), pointing to a prominent role of the glycolysis pathway in cell growth. However, a potential contribution of the pentose phosphate pathway to *Abca1*$^{-/-}$*Abcg1*$^{-/-}$ leukocyte proliferation could not be completely excluded from this experiment. We next challenged the mitochondria with either

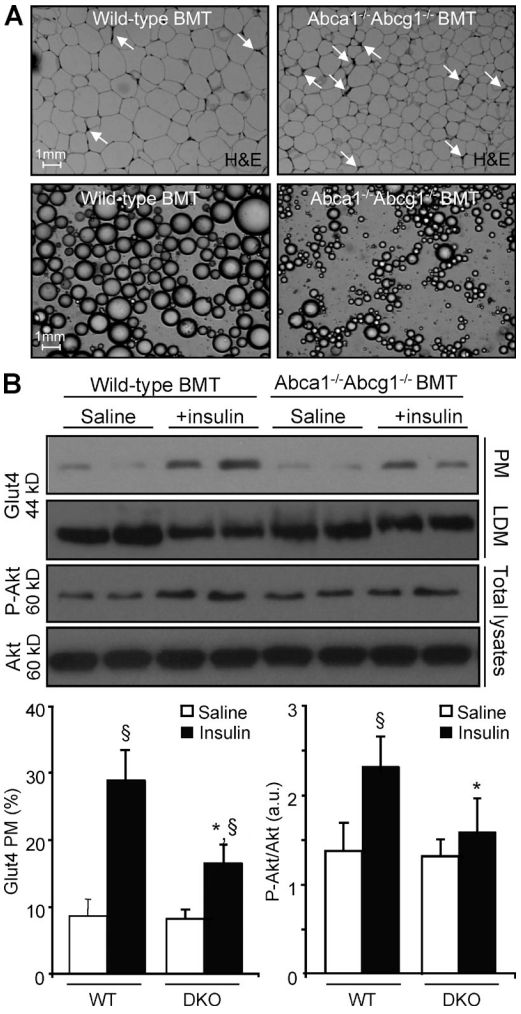

Figure 2. Infiltrated leukocytes modulate adipose tissue insulin sensitivity in *Abca1*$^{-/-}$*Abcg1*$^{-/-}$ BM chimeras. (A) Paraffin-embedded serial sections obtained from the adipose tissue of WT and *Abca1*$^{-/-}$*Abcg1*$^{-/-}$ BM transplanted (BMT) mice fed a chow diet. Representative H&E staining revealed an extensive myeloid cell infiltrate in *Abca1*$^{-/-}$*Abcg1*$^{-/-}$ BM transplanted mice compared with controls. Micrographs of isolated epididymal adipose cells confirmed reduced adipose cell size in *Abca1*$^{-/-}$*Abcg1*$^{-/-}$ BM transplanted mice. Data representative of four to six animals per group are shown. Bars, 1 mm. (B) Western blot analysis of plasma membrane (PM) and low-density microsome (LDM) Glut4, phospho-Akt, and total Akt in the adipose tissue of WT and *Abca1*$^{-/-}$*Abcg1*$^{-/-}$ BM transplanted mice after acute i.p. injection of an insulin bolus. Quantitative results were obtained from two independent experiments. Values are mean ± SEM and expressed as percent expression of PM Glut4 over HDM fraction or as arbitrary units (a.u.). *, $P < 0.05$ versus insulin-injected WT controls; §, $P < 0.05$ versus saline-injected mice.

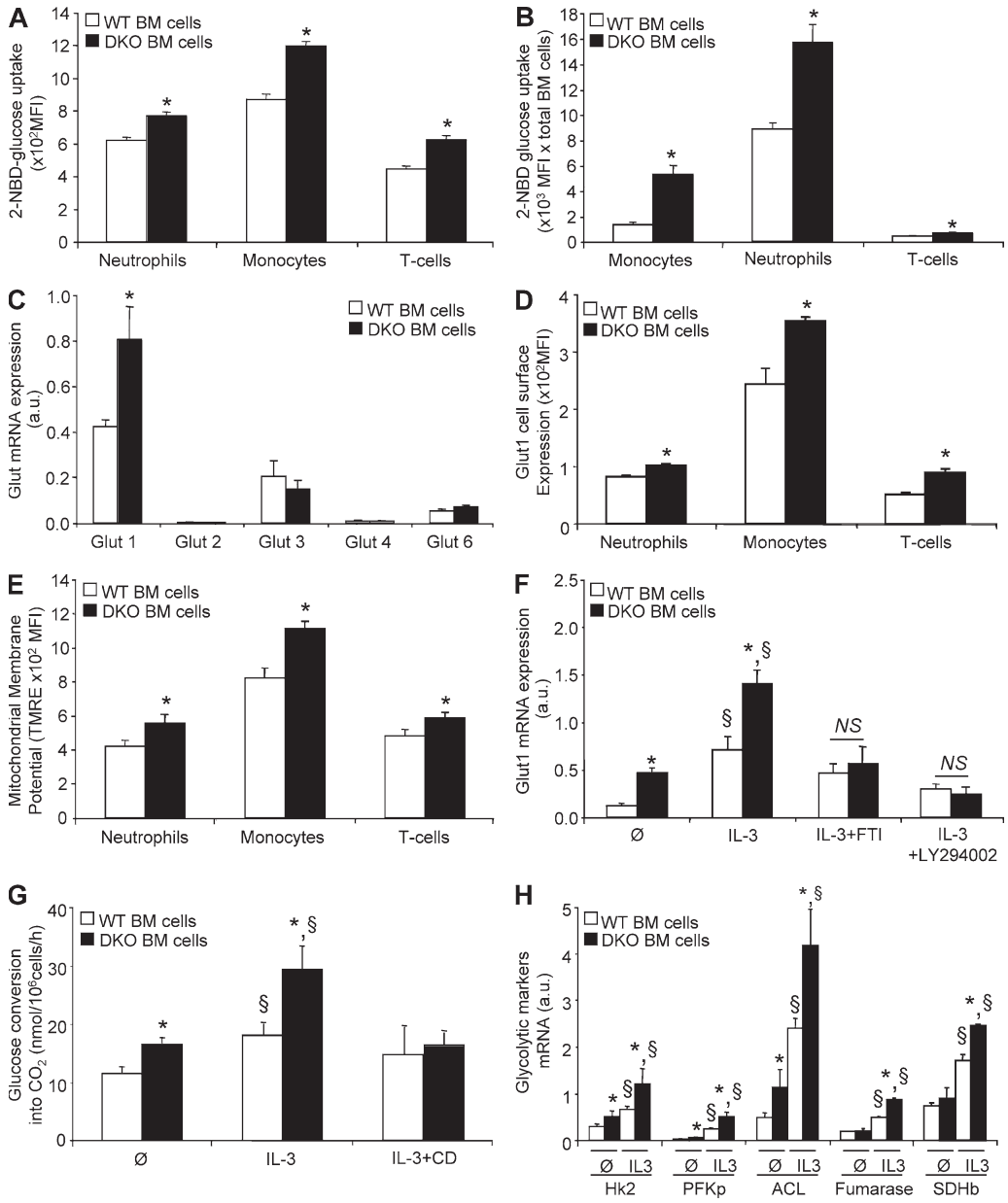

Figure 3. Enhanced glycolytic activity in *Abca1*$^{-/-}$*Abcg1*$^{-/-}$ leukocytes. (A) Ex vivo characterization of the glucose binding and/or uptake in WT and *Abca1*$^{-/-}$*Abcg1*$^{-/-}$ BM leukocyte subpopulations (i.e., CD115^{+} monocytes, CD115^{-}Grl^{+} neutrophils, and TCRb^{+} lymphocytes) using a fluorescent D-glucose analogue (2-NBDG). (B) Glucose uptake normalized by the amount of BM leukocytes. (C) mRNA expression of glucose transporters (Gluts) in freshly isolated WT and *Abca1*$^{-/-}$*Abcg1*$^{-/-}$ BM cells. (D) Cell surface expression of Glut1 was also quantified in WT and *Abca1*$^{-/-}$*Abcg1*$^{-/-}$ BM neutrophils, monocytes, and lymphocytes. (E) Mitochondrial membrane potential measured by fluorescent TMRE dye. All results are means ± SEM and are representative of two independent experiments (n = 5–6 animals per groups). *, P < 0.05 versus controls. MFI, mean fluorescence intensity. (F) Glut1 expression after BM cells were treated for 72 h with the indicated growth factors and in the presence or absence of 1 µM farnesyl transferase inhibitor (FTI) or 10 µM PI3K inhibitor (LY294002). Values were normalized to ribosomal 18S. (G) Effect of IL-3 treatment and cholesterol depletion by cyclodextrin (CD) on [^{14}C]glucose conversion into CO_2 in WT and *Abca1*$^{-/-}$*Abcg1*$^{-/-}$ BM cells. (H) mRNA expression of Hk2, PFK isoform p (PFKp), ACL, fumarase, and SDH subunit b (SDHb) in WT and *Abca1*$^{-/-}$*Abcg1*$^{-/-}$ BM-derived cells untreated or treated for 72 h with IL-3. Values were normalized to ribosomal 18S. Results are means ± SEM of cultures from three independent mice. *, P < 0.05 versus WT controls; §, P < 0.05 versus untreated condition.

branched-chain amino acids (i.e., valine, leucine, and isoleucine) or with cysteamine to fuel the tricarboxylic acid (TCA) cycle with acetyl-coA or coA, respectively, but these treatments did not increase the proliferation of *Abca1*$^{-/-}$*Abcg1*$^{-/-}$ leukocytes, suggesting the requirement of the pyruvate entry into the TCA cycle for proliferation (Fig. 4 G). We next used the phosphoserine phosphatase inhibitor DL-AP3 (Hawkinson et al., 1996), which blocks the rate-limiting step of the serine

biosynthetic pathway (Lunt and Vander Heiden, 2011) but also the pyruvate dehydrogenase phosphoserine phosphatases (PDPs) known to switch metabolic flux from glycolysis toward oxidative phosphorylation. This treatment prevented the enhanced proliferation of *Abca1*$^{-/-}$*Abcg1*$^{-/-}$ leukocytes (Fig. 4 G). Because inhibition of serine palmitoyltransferase by myriocin, downstream of the serine biosynthetic pathway, proportionately inhibited both WT and *Abca1*$^{-/-}$*Abcg1*$^{-/-}$ leukocytes (Fig. 4 G), this suggested that the effect of DL-AP3 was most likely related to inhibition of PDPs. Inhibition of diglyceride acyltransferase also proportionately inhibited both WT and *Abca1*$^{-/-}$*Abcg1*$^{-/-}$ leukocyte proliferation (Fig. 4 G), suggesting that despite enhanced lipid synthesis (Fig. 5 A), neither ceramide or triglyceride biosynthesis was the limiting step for the proliferation of these cells.

Proliferating *Abca1*$^{-/-}$*Abcg1*$^{-/-}$ leukocytes exhibit enhanced mitochondrial metabolism

To better understand the contribution of the mitochondrial metabolism, we next assessed the ability of *Abca1*$^{-/-}$*Abcg1*$^{-/-}$ leukocytes to proliferate after treatment with membrane-permeable antioxidants. Although glutathione monoethyl ester partially reduced the proliferation of all cells, tempol abrogated the enhanced proliferation of *Abca1*$^{-/-}$*Abcg1*$^{-/-}$ leukocytes (Fig. 4 H). Recently, Samudio et al. (2010) proposed that leukemia cells uncouple fatty acid oxidation from ATP synthesis and rely on de novo fatty acid synthesis to support fatty acid oxidation. Consistent with this observation, pharmacological inhibition of carnitine palmitoyltransferase I (CPT-1) with etomoxir prevented the hyperproliferative response of *Abca1*$^{-/-}$*Abcg1*$^{-/-}$ leukocytes (Fig. 4 H). Finally, carnitine supplementation of the cells to promote mitochondrial efflux of excess acetyl moieties from both glucose and fat oxidation (Muoio et al., 2012) prevented the higher proliferation rate of *Abca1*$^{-/-}$*Abcg1*$^{-/-}$ leukocytes (Fig. 4 H), providing additional evidence that the mitochondrial metabolism was responsible for the enhanced proliferation in *Abca1*$^{-/-}$*Abcg1*$^{-/-}$ leukocytes. Together, these findings showed that *Abca1*$^{-/-}$*Abcg1*$^{-/-}$ BM cells directed the available glucose toward oxidative phosphorylation (Fig. 4 I), which could explain the enhanced glucose oxidation observed in *Abca1*$^{-/-}$*Abcg1*$^{-/-}$ BM transplanted mice (Fig. 1 E).

Glut1 inhibition prevents both IL-3–mediated myeloid proliferation and TLR4-mediated macrophage inflammatory response

The increased glucose conversion into lipids at basal or after IL-3 activation in *Abca1*$^{-/-}$*Abcg1*$^{-/-}$ leukocytes was abolished by Fasentin, a Glut1 inhibitor (Fig. 5 A; Wood et al., 2008), as was the proliferation of these cells (Fig. 5 B). Together, these findings suggest that IL-3Rβ subunit signaling enhances the Glut1-dependent glucose uptake of *Abca1*$^{-/-}$*Abcg1*$^{-/-}$ leukocytes to promote their proliferation. Enhanced glucose consumption and Glut1 expression were previously observed in macrophages during inflammatory responses (Fukuzumi et al., 1996; Gamelli et al., 1996). Consistent with the previously observed enhancement in Toll-like receptor signaling in *Abca1*$^{-/-}$*Abcg1*$^{-/-}$ macrophages (Yvan-Charvet et al., 2008), analysis of the rates of [^{14}C]glucose oxidation in vitro in BM-derived macrophages revealed that in basal and LPS-stimulated conditions, *Abca1*$^{-/-}$*Abcg1*$^{-/-}$ macrophages exhibited a higher glucose consumption that was associated with increased Glut1 mRNA levels (not depicted). Interestingly, Glut1 inhibition by Fasentin reduced the inflammatory response induced by LPS in *Abca1*$^{-/-}$*Abcg1*$^{-/-}$ macrophages (Fig. 5 C). Although the mRNA levels of Hk2 and glucose-6-phosphate dehydrogenase followed the inflammatory pattern (Fig. 5 D), glycolytic genes such as PFK and ACL were barely affected by LPS in either WT or *Abca1*$^{-/-}$*Abcg1*$^{-/-}$ macrophages (Fig. 5 D). This contrasted with proliferating *Abca1*$^{-/-}$*Abcg1*$^{-/-}$ leukocytes (Fig. 4 I). Thus, *Abca1*$^{-/-}$*Abcg1*$^{-/-}$ macrophages could contribute not only to the enhanced glucose oxidation observed in *Abca1*$^{-/-}$*Abcg1*$^{-/-}$ BM transplanted mice (Fig. 1 E), but also to the local adipose tissue insulin resistance mediated by enhanced inflammatory response (Fig. 2 B). Together, these findings revealed that Glut1 controls both the proliferative and inflammatory status of *Abca1*$^{-/-}$*Abcg1*$^{-/-}$ leukocytes.

Both Glut1 inhibition and ApoA-I overexpression prevent fat loss in *Abca1*$^{-/-}$*Abcg1*$^{-/-}$ BM transplanted mice

We next explored the in vivo relevance of reducing the proliferation and inflammatory status of myeloid cells through Glut1 inhibition on the adipose tissue loss of *Abca1*$^{-/-}$*Abcg1*$^{-/-}$ BM chimeras. Mice that received WT or *Abca1*$^{-/-}$*Abcg1*$^{-/-}$ BM transduced with lentiviruses encoding Glut1 shRNA exhibited a 1.6-fold reduction in Glut1 mRNA expression (not depicted) and a 20–30% reduction in the cell surface expression of Glut1 in their BM cells 7 wk after reconstitution, and this was sufficient to normalize the Glut1 cell surface expression to WT levels in *Abca1*$^{-/-}$*Abcg1*$^{-/-}$ BM transplanted mice (Fig. 5 E). This was associated with normalization of the 2-NBDG uptake in *Abca1*$^{-/-}$*Abcg1*$^{-/-}$ BM leukocytes (Fig. 5 F) and with normalization of the leukocyte counts in these mice (Fig. 5 G). Remarkably, the adipose tissue loss of mice transplanted with *Abca1*$^{-/-}$*Abcg1*$^{-/-}$ BM was rescued by transduction with Glut1 shRNA lentiviral particles (Fig. 5 H). We previously reported that the myeloproliferative syndrome and inflammatory phenotype of *Abca1*$^{-/-}$*Abcg1*$^{-/-}$ BM chimeras was reversed by overexpression of the human apoA-I transgene (ApoA-I^{Tg}; Yvan-Charvet et al., 2008, 2010). We now show that overexpression of the human apoA-I transgene also reversed fat loss in *Abca1*$^{-/-}$*Abcg1*$^{-/-}$ BM transplanted mice (Fig. 5 I). Additionally, the apoA-I transgene normalized Glut1 cell surface expression in *Abca1*$^{-/-}$*Abcg1*$^{-/-}$ BM cells (Fig. 5 J). Together, our results suggest that suppression of Glut1 in myeloproliferative disorders may represent a novel approach not only to treat leukocytosis but also associated adipose tissue loss. Additionally, we now show that the rescue of the myeloproliferative disease of *Abca1*$^{-/-}$*Abcg1*$^{-/-}$ BM chimeras by overexpression of the human apoA-I transgene

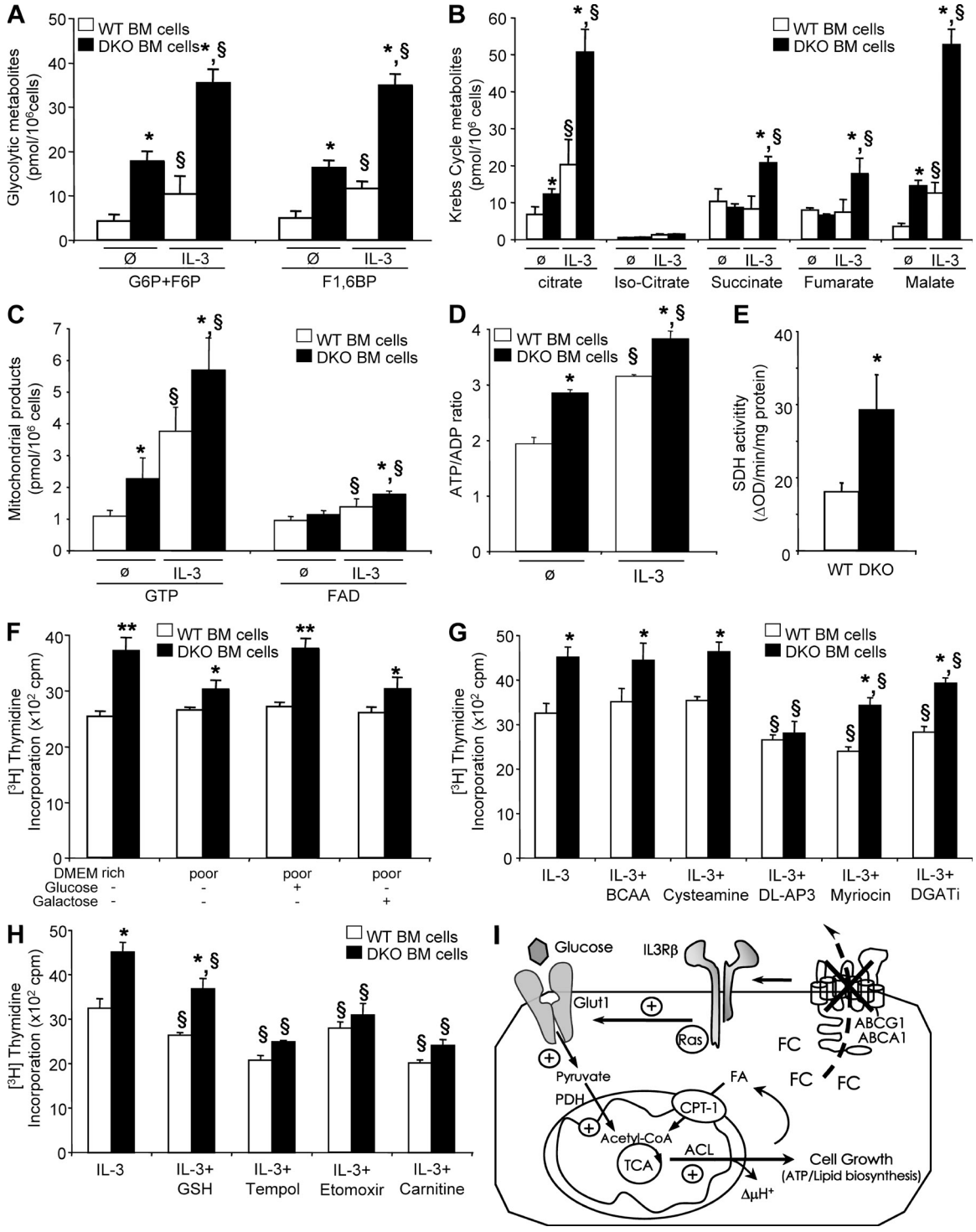

Figure 4. The IL-3Rβ–dependent proliferation of *Abca1*$^{-/-}$*Abcg1*$^{-/-}$ leukocytes is driven by increased mitochondrial metabolism. (A–D) Effect of IL-3 treatment on glycolytic metabolites (glucose 6-phosphate/fructose 6-phosphate and fructose 1,6-diphosphate; A), citric acid metabolites (B), related mitochondrial products (GTP and FAD; C), and ATP/ADP ratio (D) in WT and *Abca1*$^{-/-}$*Abcg1*$^{-/-}$ BM cells determined by LC-MS. (E) SDH activity in these cells. Results are means ± SEM of cultures from three independent mice. *, $P < 0.05$ versus WT controls; §, $P < 0.05$ versus treatment. (F) WT and *Abca1*$^{-/-}$*Abcg1*$^{-/-}$ BM cells were grown for 48 h in 20 mM glucose DMEM (DMEM rich) or low-glucose DMEM (DMEM poor) supplemented with 20 mM glucose or 20 mM galactose in the presence of IL-3. Proliferation rates were determined after 2-h [^{3}H]thymidine pulse labeling. (G and H) BM cells were grown for 48 h in liquid culture containing 10% FBS IMDM in the presence of the indicated chemical compounds and IL-3. Proliferation rates were determined after 2-h [^{3}H]thymidine pulse labeling. Results are means ± SEM of an experiment performed in triplicate. *, $P < 0.05$ versus WT controls; §, $P < 0.05$ versus untreated condition. BCAA, branched-chain amino acids; DGATi, diglyceride acyltransferase inhibitor.

(Yvan-Charvet et al., 2010) was in part associated with reduced Glut1 levels on leukocytes and prevented their adipose loss.

ApoA-I overexpression prevents the increased glucose oxidation and adipose tissue atrophy in Flt3-ITD and Mpl-W515L mutant–mediated myeloproliferative disorders

As altered high-density lipoprotein (HDL) cholesterol homeostasis has been previously observed in myeloproliferative disorders (Fiorenza et al., 2000; Westerterp et al., 2012), we further tested whether the increased glucose oxidation and associated adipose tissue atrophy observed in *Abca1*$^{-/-}$*Abcg1*$^{-/-}$ BM transplanted mice could be observed as a more general phenotype in other mouse models of myeloproliferative disorders and whether overexpression of the human apoA-I transgene would still be an efficient therapeutic in these models. The Flt3-ITD and Mpl-W515L alleles have been identified in patients with acute myeloid leukemia and myelofibrosis, respectively, and confer a fully penetrant myeloproliferative disorder in mice (Kelly et al., 2002; Pikman et al., 2006). Accordingly, mice that received BM transduced with retroviruses encoding Flt3-ITD or Mpl-W515L exhibited massive myeloid expansion compared with control retrovirus (Fig. 6, A and B), an effect which was partially reversed by overexpression of the human ApoA-I transgene (Fig. 6, A and B). We also observed epididymal fat mass atrophy and reduced plasma leptin levels in both models (Fig. 6 C and not depicted, respectively). Massive leukocyte infiltration was also observed in their adipose tissue (not depicted). Similar to *Abca1*$^{-/-}$*Abcg1*$^{-/-}$ BM transplanted mice, these features were associated with an increased RQ during the dark phase (Fig. 6, D and E), reflecting an ∼20% increase in glucose oxidation during this period (Fig. 6 F). Interestingly, Mpl-W515L and Flt3-ITD mutant leukocytes exhibited a significant increase in Glut1 cell surface expression (Fig. 6 G). Remarkably, overexpression of the human ApoA-I transgene not only prevented the fat mass loss (Fig. 6 C) of mice bearing the Mpl-W515L and Flt3-ITD mutations, but also significantly reversed the increased Glut1 cell surface expression in Mpl-W515L and Flt3-ITD leukocytes (Fig. 6 G) that was associated with increased RQ (Fig. 6, H and I) and glucose oxidation during the feeding period (Fig. 6 F).

DISCUSSION

Although there is growing evidence that weight loss, and especially the loss of muscle and adipose tissue mass, is a hallmark of chronic inflammatory diseases such as chronic infection, cancer, and heart failure (Delano and Moldawer, 2006), the underlying mechanisms remain poorly understood, leading to a lack of effective therapy. Most of the emerging therapeutic approaches to prevent adipose tissue loss focus on reducing the elevated circulating cytokine levels (Argilés et al., 2011) in part because of their action on insulin resistance and fat mobilization (Delano and Moldawer, 2006; Das et al., 2011). However, traditional antiinflammatory approaches such as COX-2 inhibitors showed for instance limited effectiveness in reversing the metabolic abnormalities seen in cancer patients (Kumar et al., 2010). Thus, there is a crucial need to better understand the mechanisms of adipose loss in this state of chronic hypermetabolism. Using three different mouse models of myeloproliferative disorders, including two models based on expression of human leukemia disease alleles (Flt3-ITD and Mpl-W515L), we uncovered a glucose steal mechanism by which proliferating and inflammatory myeloid cells take up and oxidize glucose during the feeding period, contributing to energy dissipation and subsequent loss of adipose mass. This reflected in part increased numbers of proliferating myeloid cells and tissues infiltrated with inflammatory myeloid cells.

Although only partially understood, there is a relationship between leukemia-causing genes and cellular energy metabolism as the survival and proliferation of leukemic cells may require glucose for de novo lipid biosynthesis (DeBerardinis et al., 2008; Lunt and Vander Heiden, 2011). The increased glucose utilization in hyperproliferating *Abca1*$^{-/-}$*Abcg1*$^{-/-}$ BM myeloid cells resulted in part from a Ras-dependent upregulation of Glut1 expression in response to enhanced IL-3 signaling (Flier et al., 1987; Yvan-Charvet et al., 2010). Similarly, Mpl and Flt3 are receptor tyrosine kinases coupled to Ras signaling, and activating mutations in these receptors (Kelly et al., 2002; Pikman et al., 2006) were shown to cause higher Glut1 expression. In this context, it is tempting to parallel our myeloproliferative mouse models with other cancer models in which malignant cells rely on high levels of aerobic glycolysis as the major source of ATP to fuel cellular proliferation, known as the Warburg effect (Vander Heiden et al., 2009). However, the classical view of the Warburg effect, which involves defect in mitochondrial oxidative phosphorylation, has been recently challenged, and mitochondrial metabolism may indeed be functional in different types of tumor cells (Jose et al., 2011). We now provide both in vitro and in vivo evidence for increased mitochondrial potential in leukocytes of our mouse

(I) Scheme illustrating the induction of glycolysis through modulation of plasma membrane cholesterol by ABCA1 and ABCG1 deficiency and increased mitochondrial metabolism that produces ATP and synthesizes lipids for cell growth. Lack of these transporters promotes growth factors dependent on IL-3Rβ signaling–mediated glycolysis as reflected by (a) enhanced Hk2 and PFKp mRNA expression, (b) enhanced glycolytic metabolites content, (c) enhanced glucose oxidation (i.e., conversion into CO_2), and (d) reversal of enhanced glucose oxidation by removal of cellular cholesterol by cyclodextrin. The pyruvate generated through glycolysis is directed into the TCA cycle and increases mitochondrial metabolism as reflected by (a) enhanced mRNA expression of fumarase and SDHb, (b) enhanced SDH activity, (c) enhanced mitochondrial metabolites and mitochondrial membrane potential ($\Delta\mu H^+$), and (d) enhanced ATP/ADP ratio. Increased lipid synthesis was also observed in *Abca1*$^{-/-}$*Abcg1*$^{-/-}$ BM cells as reflected by (a) enhanced mRNA expression of ACL and (b) enhanced glucose conversion into lipids.

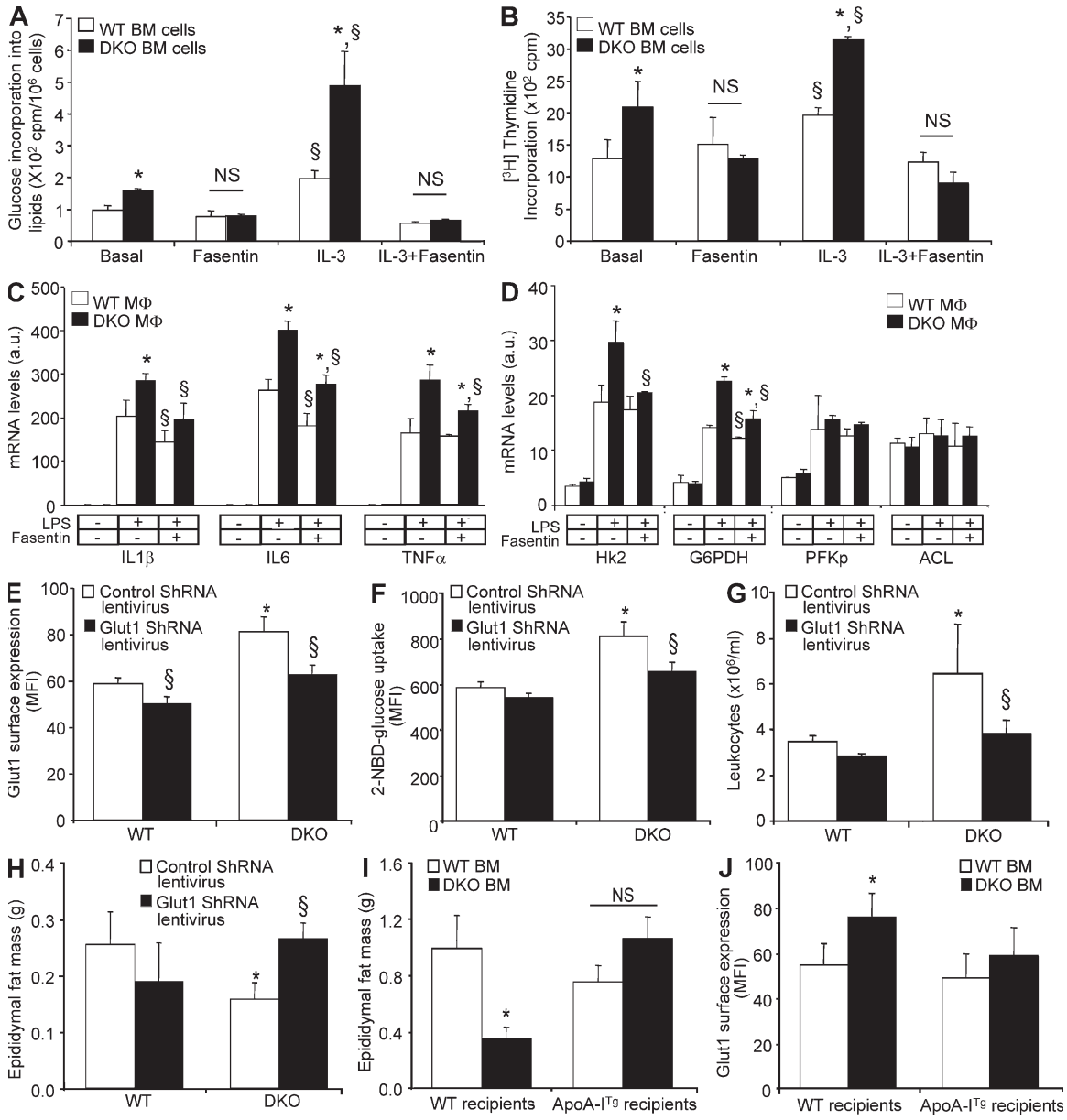

Figure 5. Inhibition of Glut1 or overexpression of the human apoA-I transgene rescues adipose atrophy in *Abca1*$^{-/-}$*Abcg1*$^{-/-}$ BM chimeras. (A) Effect of IL-3 treatment on [^{14}C]glucose conversion into lipids in WT and *Abca1*$^{-/-}$*Abcg1*$^{-/-}$ BM cells in the presence or absence of 50 µM fasentin, a Glut1 inhibitor. (B) Effect of Fasentin on IL-3–mediated proliferation in WT and *Abca1*$^{-/-}$*Abcg1*$^{-/-}$ BM cells. (C and D) Effect of Fasentin on LPS-mediated inflammatory (C) and glycolytic (D) responses in WT and *Abca1*$^{-/-}$*Abcg1*$^{-/-}$ BM-derived macrophages. Values were normalized to ribosomal 18S. Results are means ± SEM of three independent experiments performed in triplicate. *, $P < 0.05$ versus WT mice; §, $P < 0.05$ versus LPS treatment. (E and F) Quantification of Glut1 cell surface expression (E) and 2-NBDG uptake by flow cytometry (F) in CD45$^+$ leukocytes isolated from the BM of WT recipients mice transplanted with WT or *Abca1*$^{-/-}$*Abcg1*$^{-/-}$ BM transduced with a lentivirus encoding Glut1 shRNA 7 wk after reconstitution. (G and H) Peripheral leukocyte counts (G) and epididymal fat mass (H) of these mice at the end of the experiment. (I and J) Histograms showing epididymal fat mass loss (I) and Glut1 cell surface expression (J) in CD45$^+$ peripheral leukocytes in chow-fed transgenic recipient mice overexpressing the human apoA-I transgene transplanted with *Abca1*$^{-/-}$*Abcg1*$^{-/-}$ BM. Results are ± SEM of an experiment of four to six animals per group. *, $P < 0.05$ versus WT recipients transplanted with WT BM; §, $P < 0.05$ versus control retrovirus. MFI, mean fluorescence intensity.

model of myeloproliferative disorder. Surprisingly, not only inhibition of PDPs but also inhibition of CPT-1 prevented the proliferation of *Abca1*$^{-/-}$*Abcg1*$^{-/-}$ leukocytes. This emphasizes a scenario in which high rates of aerobic glycolysis in leukemia cells are necessary to support the mitochondrial metabolism of fatty acids (i.e., fats burn in the fire of carbohydrates; Samudio et al., 2010). Although the mechanisms orchestrating this phenomenon remain to be investigated, it appears unlikely to be mediated by triglyceride or ceramide biosynthesis. Interestingly, the antiproliferative effect

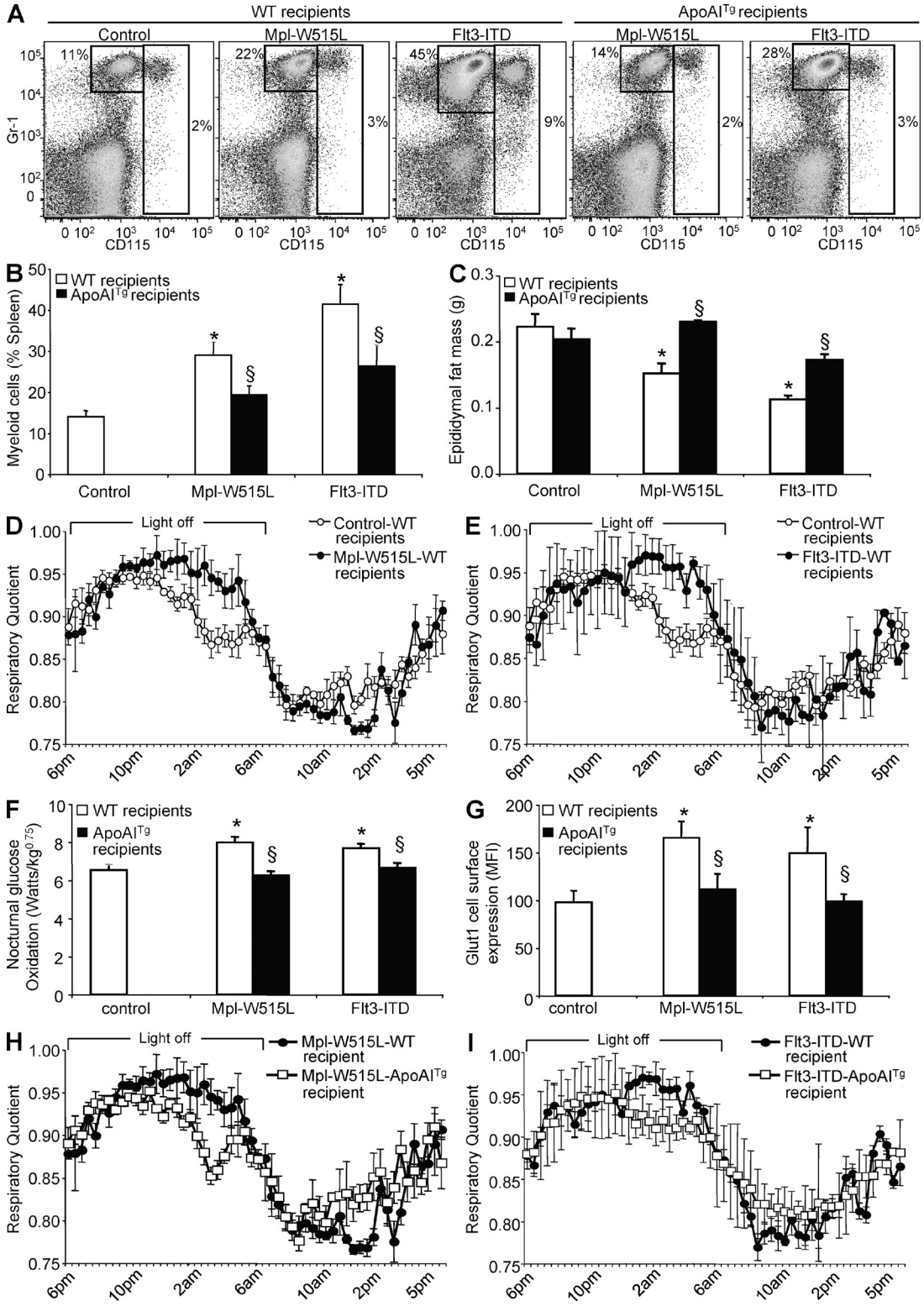

Figure 6. HDL prevents the adipose tissue atrophy and enhanced glucose oxidation caused by Mpl-W515L and Flt3-ITD activating mutations. (A) Representative dot plots and quantification of the splenic myeloid cells ($CD115^+$ monocytes and $CD115^-Gr1^+$ neutrophils) of WT and ApoA-I transgenic recipient mice transplanted with Mpl-W515L– and Flt3-ITD–transduced BM cells. (B and C) Quantification of the myeloid cells (B) and epididymal fat mass (C) of these mice. (D, E, F, H, and I) RQ measured by indirect calorimetry (D, E, H, and I) and quantification of the nocturnal glucose oxidation of these mice (F). (G) Quantification of the cell surface expression of Glut1 in $CD45^+$ leukocytes of these mice. Results are mean ± SEM of an experiment of four to five animals per group. *, $P < 0.05$ versus control mice; §, $P < 0.05$ versus respective WT recipients. MFI, mean fluorescence intensity.

of carnitine suggested that prevention of oxidative phosphorylation by efflux of excess mitochondrial acetyl moieties (Muoio et al., 2012) might represent a novel strategy for the treatment of hematological malignancies. In conclusion, increased glucose oxidation and mitochondrial metabolism–dependent proliferation of myeloid cells likely contributed to energy dissipation and subsequent loss of adipose mass.

Leukocytes and adipocytes can communicate through interaction between secreted inflammatory cytokines and their cognate receptors (Lumeng and Saltiel, 2011; Odegaard and Chawla, 2011). The finding that highly infiltrated adipose depots were associated with impaired Glut4 translocation to the plasma membrane in response to insulin in *Abca1*$^{-/-}$ *Abcg1*$^{-/-}$ BM chimeras was strongly implied by prior studies indicating insulin resistance in peripheral tissues secondary to increased tumor-derived cytokines (Delano and Moldawer, 2006). Nevertheless, these findings provide strong evidences that local inflammation driving adipose tissue insulin resistance is not restricted to a role on fat mobilization in cancer-associated adipose tissue loss (Das et al., 2011). This suggests that myeloproliferative cells develop efficient strategies to divert glucose from its expected destination, i.e., fat storage as a mean to meet their energetic needs. In part, this could be related to a shunt of glucose to the pentose phosphate pathway that has been recently shown to modulate the inflammatory response of activated immune cells (Ham, M., et al. 2008. *The FASEB Journal* Meeting. Abstr. 615.1; Blagih and Jones, 2012). This could ultimately contribute not only to the enhanced glucose oxidation observed in our mouse models of myeloproliferative disorders but also to the local adipose tissue insulin resistance mediated by enhanced inflammatory response.

Finally, we showed that Glut1 blockade prevented both basal and IL-3–induced proliferation of *Abca1*$^{-/-}$*Abcg1*$^{-/-}$ leukocytes in vitro and prevented LPS-induced inflammatory cytokine response in *Abca1*$^{-/-}$*Abcg1*$^{-/-}$ macrophages. This translated in vivo into the rescue of leukocytosis and adipose tissue infiltration of *Abca1*$^{-/-}$*Abcg1*$^{-/-}$ BM transplanted mice in response to Glut1 inhibition. Remarkably, this prevented the adipose tissue loss of these mice, confirming the key role of myeloid Glut1 in the diversion of energy stores from adipose to myeloid cells. Similarly, overexpression of the human ApoA-I transgene, previously shown to raise plasma HDL levels and prevent the myeloproliferative syndrome of *Abca1*$^{-/-}$*Abcg1*$^{-/-}$ BM transplanted mice (Yvan-Charvet et al., 2010), reduced Glut1 cell surface expression in leukocytes and prevented their fat loss. This reflected in part the removal of excess cholesterol from plasma membrane in *Abca1*$^{-/-}$*Abcg1*$^{-/-}$ myeloid cells that prevented the IL-3Rβ signaling (Yvan-Charvet et al., 2010) and subsequent increase in Glut1-dependent glucose uptake (Fig. 3 G). These findings were further extended in two mouse models of myeloproliferative disorders based on expression of human leukemia disease alleles (Flt3-ITD and Mpl-W515L) in which overexpression of the human ApoA-I transgene reduced myeloid expansion, decreased cell surface expression of Glut1 in leukocytes, reduced glucose oxidation during the feeding period, and prevented adipose tissue loss.

In conclusion, our study elucidates a glucose steal mechanism by proliferating and inflammatory myeloid cells that contributes to depletion of adipose tissue in myeloproliferative disorders. This mechanism involved enhanced glucose oxidation by myeloid cells that led to energy dissipation with consequences on fat storage. Inhibition of glucose uptake by leukocytes with a Glut1 inhibitor or by treatments that increase HDL levels could ultimately provide new therapeutic approaches not only to limit cell proliferation but also to prevent the energy imbalance and fat atrophy observed in myeloproliferative disorders and in other human malignancies.

MATERIALS AND METHODS

Mice and treatments. WT, *Abca1*$^{-/-}$, *Abcg1*$^{-/-}$, and *Abca1*$^{-/-}$*Abcg1*$^{-/-}$ littermates in a mixed C57BL/6 × DBA background (Yvan-Charvet et al., 2007) were used for this study. Human apoA-1 transgenic (hapoA-1^{Tg}) mice were obtained from the Jackson Laboratory. BM transplantation into the genetically uniform F1 generation obtained by crossing C57BL/6 WT, hapoA-1^{Tg} mice with WT DBA mice (The Jackson Laboratory) was performed as previously described (Yvan-Charvet et al., 2007). Animal protocols were approved by the Institutional Animal Care and Use Committee of Columbia University. Animals had ad libitum access to both food and water.

HSC transplantation. HSC transplantation was adapted from a previously described protocol (Wagers et al., 2002). In brief, congenic CD45.1$^+$ B6.SJL-Ptprca—Pep3b-/BoyJ were purchased from the Jackson Laboratory and used to isolate Sca-1–depleted BM cells by FACS sorting. HSCs were isolated by FACS sorting of lineage-depleted BM from WT and *Abca1*$^{-/-}$*Abcg1*$^{-/-}$ backcrossed for 10 generations on a C57/BL6 background, based on the following cell surface markers: c-kit and Sca-1 (LSK, Lin$^-$Sca$^+$c-kit$^+$). Lethally irradiated WT recipients were i.v. injected with 10^6 cells containing a mixture of CD45.1$^+$ Sca-1–depleted BM cells and CD45.2$^+$ LSK cells from either WT or *Abca1*$^{-/-}$*Abcg1*$^{-/-}$ mice in the ratio 1:2,000. Transplanted recipients were screened by flow cytometry for reconstitution of CD45.2$^+$ leukocytes in peripheral blood at 6 wk after transplant. More than 90% of leukocytes stained for the congenic marker CD45.2, thereby confirming the engraftment of LSK cells (Wagers et al., 2002).

Retroviral BM transplantation. The retroviral BM transplant assay was performed as previously described (Pikman et al., 2006). In brief, control, Mpl-W515L and Flt3-ITD retroviral supernatants were titered and used to transduce WT BM cells. In independent experiments, premade control and Glut1 shRNA lentiviral particles (Santa Cruz Biotechnology, Inc.) were used to transduce WT and *Abca1*$^{-/-}$*Abcg1*$^{-/-}$ BM cells. BM cells were cultured for 24 h in transplantation media (RPMI + 10% FBS + 6 ng/ml IL-3, 10 ng/ml IL-6, and 10 ng/ml stem cell factor) and treated by spin infection with retroviral supernatants (1 ml supernatant per 4 × 10^6 cells in the presence of polybrene) and centrifuged at 1,800 *g* for 90 min. The spin infection was repeated 24 h later. After washing, the cells were used for BM transplantation into lethally irradiated WT recipient mice.

Energy expenditure. Metabolic activity was performed by in vivo indirect open circuit calorimetry at the Mouse Phenotyping Core of Columbia University using a CaloSys calorimetry system (TSE Systems, Inc). Animals were placed into experimental chambers with free access to food and water for a 4-d consecutive period. Food intake was recorded with an automated feeding monitor system through the study period. Constant airflow (0.5 liter/min) was drawn through the chamber and monitored by a mass-sensitive flow meter. To calculate oxygen consumption (VO_2), carbon dioxide production (VCO_2), and RQ (ratio of VCO_2 to VO_2), gas concentrations were monitored at the inlet and outlet of the scaled chambers.

Total metabolic rate (energy expenditure) was calculated from oxygen consumption and carbon dioxide production using Lusk's equation and expressed as watts per kilogram to the 0.75 power of body weight (Yvan-Charvet et al., 2005). Glucose and lipid oxidation were calculated as previously described (Yvan-Charvet et al., 2005).

In vivo 2-[^{14}C]-DG uptake. Uptake of 2-[^{14}C]-DG in peripheral tissues was measured as previously described (Rofe et al., 1988). In brief, 2 μCi 2-[^{14}C]-DG was i.v. injected, and blood samples were collected at 5, 10, 20, 30, and 40 min. Blood glucose was monitored through the study period with a glucometer (Roche). After 40 min, adipose tissue, skeletal muscle, heart, lung, spleen, and brain were rapidly dissected, weighed, and homogenized with 5% $HClO_4$ solution. BM cells were collected from leg bones, and peripheral leukocytes were obtained after RBC lysis. The radioactivity incorporated in both 2-[^{14}C]-DG and its 6-phosphate derivative was measured in the $HClO_4$ extract and expressed as total radioactivity per tissue weight. The rate constant of net tissue uptake of 2-[^{14}C]-DG was calculated as described previously (Rofe et al., 1988). In brief, the relative glucose uptake was calculated by dividing the area under the blood 2-[^{14}C]-DG disappearance curve (cpm/min/ml) to the steady-state glucose concentration (mM) multiplied by the tissue 2-[^{14}C]-DG (cpm/g tissue or cpm/10^6 cells for the BM) at 40 min.

Blood parameters. Plasma leptin and insulin were determined by ELISA (Mouse Leptin Quantikine ELISA kit [R&D Systems]; Mouse insulin ELISA kit [Crystal Chem, Inc.]). Plasma TNF was measured by Luminex assay (Cytokine Core Laboratory). Blood glucose was assayed with a glucometer (Roche).

Histopathology. Mice were euthanized in accordance with the American Veterinary Association Panel of Euthanasia. Adipose tissue was serially paraffin sectioned and stained with hematoxylin and eosin (H&E) for morphological analysis as previously described (Yvan-Charvet et al., 2007).

Adipose tissue cellularity. Cellularity of epididymal adipose tissue was determined as previously described (Yvan-Charvet et al., 2005). In brief, images of isolated adipocytes were acquired from a light microscope (IX-70; Olympus) fitted with a charge-coupled device camera (RS Photometrics), and the measurement of ~400 cell diameters was performed allowing calculation of a mean fat cell weight. Tissue triglyceride content was measured from a sample of adipose tissue using a commercial kit (Sigma-Aldrich). Fat cell number was estimated by dividing the tissue lipid content by the fat cell weight.

Glucose tolerance tests. After 6 h of fasting, mice were injected i.p. with D-glucose (2 g/kg of body weight), and blood samples were obtained by tail bleeding at 0, 15, 30, 60, 90, and 120 min after injection (Yvan-Charvet et al., 2005). Blood glucose was assayed with a glucometer (Roche).

Flow cytometry analysis. BM cells were collected from leg bones or spleen, lysed to remove RBCs, and filtered before use. Freshly isolated cells were stained with the appropriate antibodies for 30 min on ice. For peripheral blood leukocytes analysis, 100 μl blood was collected into EDTA tubes before RBC lysis, filtration, and staining for 30 min on ice. To assess the uptake of 2-NBDG, prestained peripheral blood leukocytes (Yvan-Charvet et al., 2010) were incubated with 10 μM 2-NBDG (Invitrogen) for 30 min, followed by flow cytometric detection of fluorescence produced by the cells (Zou et al., 2005). The mitochondrial membrane potential was analyzed with 25 nM fluorescent TMRE (AnaSpec) staining for 30 min on prestained leukocytes. Viable cells, gated by light scatter or exclusion of $CD45^-$ cells, were analyzed on a four-laser LSRII cell analyzer (BD) or sorted on a FACSAria Cell Sorter (BD), both running with DiVa software (BD). Data were analyzed using FlowJo software (Tree Star).

Antibodies. Anti–mouse CD45 (clone 30F11), CD115 (AFS98), TCR-β (H57-597), F4/80 (BM8), CD2 (RM2-5), CD3e (145-2C11), CD4 (GK1.5), CD8b (53-6.7), CD19 (eBio1D3), CD45R (B220, RA3-6B2), Gr-1 (Ly6G, RB6-8C5), Cd11b (Mac1, M1/70), Ter119 (Ly76) and NK1.1 (Ly53, PK136), c-Kit (CD117, ACK2), and Sca-1 (D7) were all purchased from eBioscience. Glut1-FITC antibody was purchased from R&D Systems. These antibodies were used to sort HSCs and stain for leukocytes in peripheral blood and tissues.

BM harvest and treatment. Primary BM cells were resuspended in IMDM (Gibco) containing 10% FCS (STEMCELL Technologies) and cultured for 1 h in tissue culture flasks to remove adherent cells, including macrophages. Suspended cells were then cultured for 72 h in the presence of 6 ng/ml IL-3 (R&D Systems). In some experiments, the farnesyl transferase inhibitor (EMD Millipore) was used at the final concentration of 1 μM, fasentin (Sigma-Aldrich) at 50 μM, DL-AP3 (Tocris Bioscience) at 50 μM, myriocin (Sigma-Aldrich) at 10 μM, diglyceride acyltransferase inhibitor (EMD Millipore) at 40 μM, etomoxir (Sigma-Aldrich) at 40 μM, branched-chain amino acids (leucine, isoleucine, and valine; Sigma-Aldrich) at 1 mM, glutathione monoethyl ester (EMD Millipore) at 10 mM, tempol (EMD Millipore) at 4 mM, and carnitine (Sigma-Aldrich) at 1 mM. For proliferation assays, cells were pulsed for 2 h with 2 μCi/ml [^{3}H]thymidine, and the radioactivity incorporated into the cells was determined by standard procedures using a liquid scintillation counter. In one experiment (Fig. 4 F), cells were resuspended in 20 mM glucose DMEM (DMEM rich; Gibco) or low-glucose DMEM (DMEM poor; Gibco) supplemented with 20 mM glucose or 20 mM galactose (Sigma-Aldrich) and cultured for 48 h in the presence of 6 ng/ml IL-3. SDH activity was determined by an ELISA kit according to the manufacturer's instructions (MitoSciences). BM-derived macrophages were isolated and cultured in 10% FBS in DMEM supplemented with M-CSF for 5–10 d before the experiment. Where indicated, macrophages were incubated with 100 ng/ml LPS (*Escherichia coli* 0111:B4; Sigma-Aldrich).

Glucose metabolism experiments. Isolated BM cells were cultured for 24 h with or without 6 ng/ml IL-3 and 50 μM fasentin, a Glut1 inhibitor. Where indicated, BM cells were differentiated into macrophages as described above. Cells were next incubated with 5.5 mM [^{14}C]glucose in 2% BSA Krebs-Ringer bicarbonate buffer, pH 7.4. After 2 h, the generated $^{14}CO_2$ and the ^{14}C incorporation into lipids were quantified as previously described (Yvan-Charvet et al., 2005). In some experiments, cellular cholesterol was depleted by 5 mM cyclodextrin for 1 h before growth factor treatment as previously described (Yvan-Charvet et al., 2010).

Directed metabolomic experiments. Isolated BM cells (10^6 cells) were cultured with or without 6 ng/ml IL-3 for 24 h. The next day, suspended cells were centrifuged at 1,000 rpm for 5 min, and pellets were rapidly washed (less than 10 s) with a mass spectrometry–compatible buffer (150 mM ammonium acetate solution) to prevent the presence of sodium and phosphate in the residue and limit interference with LC-MS analyses. After a second step of centrifugation, pellets were immediately frozen in liquid nitrogen to quench metabolism according to the University of Michigan Molecular Phenotyping Core facility's instructions. Samples were shipped on dry ice to the Molecular Phenotyping Core facility where metabolites were extracted by exposing the cells to a chilled mixture of 80% methanol, 10% chloroform, and 10% water. Glycolytic and citric acid metabolites were then analyzed by the Molecular Phenotyping Core facility using LC-MS as previously described (Yuneva et al., 2012).

Western blot analysis. 2-h-fasted mice were administrated insulin i.p. (0.4 U/mouse). After 5 min, freshly isolated adipose tissue was homogenized as previously described (Yvan-Charvet et al., 2005), and cell extracts were either directly used to measure phospho-Akt (clone 587F11; Cell Signaling Technology) by Western blot analysis or fractionated by differential centrifugation to isolate plasma membranes and low-density microsomes (Yvan-Charvet et al., 2010) and quantify Glut4 expression (clone 1F8; R&D Systems).

RNA analysis. Total RNA extraction, cDNA synthesis, and real-time PCR were performed as described previously (Yvan-Charvet et al., 2005). Ribosomal 18S RNA expression was used to account for variability in the initial quantities of mRNA.

Statistical analysis. Statistical significance was performed by two-tailed parametric Student's *t* test or by one-way ANOVA (four-group comparisons) with a Bonferroni multiple comparison post test (GraphPad Software).

We thank Dr. Kristie Gordon for assistance with flow cytometry, Pr. Pascal Ferre for scientific discussion, and the French Cancer Research Association (ARC).

This work utilized Core Services supported by a National Institutes of Health (NIH) grant (DK089503) to the University of Michigan. This work was supported by grants to L. Yvan-Charvet from the American Heart Association (SDG2160053), to E.L. Gautier from the American Heart Association (10POST4160140), to M. Westerterp from the Netherlands Organization of Sciences (NWO VENI grant 916.11.072), to G.J. Randolph from the NIH (AI061741), and to A.R. Tall from the NIH (HL54591).

The authors have no financial conflict with these experiments.

Submitted: 22 June 2012
Accepted: 10 December 2012

REFERENCES

Argilés, J.M., S. Busquets, and F.J. López-Soriano. 2011. Anti-inflammatory therapies in cancer cachexia. *Eur. J. Pharmacol.* 668:S81–S86. http://dx.doi.org/10.1016/j.ejphar.2011.07.007

Blagih, J., and R.G. Jones. 2012. Polarizing macrophages through reprogramming of glucose metabolism. *Cell Metab.* 15:793–795. http://dx.doi.org/10.1016/j.cmet.2012.05.008

Bustamante, E., and P.L. Pedersen. 1977. High aerobic glycolysis of rat hepatoma cells in culture: role of mitochondrial hexokinase. *Proc. Natl. Acad. Sci. USA.* 74:3735–3739. http://dx.doi.org/10.1073/pnas.74.9.3735

Chang, F., J.T. Lee, P.M. Navolanic, L.S. Steelman, J.G. Shelton, W.L. Blalock, R.A. Franklin, and J.A. McCubrey. 2003. Involvement of PI3K/Akt pathway in cell cycle progression, apoptosis, and neoplastic transformation: a target for cancer chemotherapy. *Leukemia.* 17:590–603. http://dx.doi.org/10.1038/sj.leu.2402824

Das, S.K., S. Eder, S. Schauer, C. Diwoky, H. Temmel, B. Guertl, G. Gorkiewicz, K.P. Tamilarasan, P. Kumari, M. Trauner, et al. 2011. Adipose triglyceride lipase contributes to cancer-associated cachexia. *Science.* 333:233–238. http://dx.doi.org/10.1126/science.1198973

DeBerardinis, R.J., J.J. Lum, G. Hatzivassiliou, and C.B. Thompson. 2008. The biology of cancer: metabolic reprogramming fuels cell growth and proliferation. *Cell Metab.* 7:11–20. http://dx.doi.org/10.1016/j.cmet.2007.10.002

Delano, M.J., and L.L. Moldawer. 2006. The origins of cachexia in acute and chronic inflammatory diseases. *Nutr. Clin. Pract.* 21:68–81. http://dx.doi.org/10.1177/011542650602100168

Dingli, D., R.A. Mesa, and A. Tefferi. 2004. Myelofibrosis with myeloid metaplasia: new developments in pathogenesis and treatment. *Intern. Med.* 43:540–547. http://dx.doi.org/10.2169/internalmedicine.43.540

Fiorenza, A.M., A. Branchi, and D. Sommariva. 2000. Serum lipoprotein profile in patients with cancer. A comparison with non-cancer subjects. *Int. J. Clin. Lab. Res.* 30:141–145. http://dx.doi.org/10.1007/s005990070013

Flier, J.S., M.M. Mueckler, P. Usher, and H.F. Lodish. 1987. Elevated levels of glucose transport and transporter messenger RNA are induced by ras or src oncogenes. *Science.* 235:1492–1495. http://dx.doi.org/10.1126/science.3103217

Fukuzumi, M., H. Shinomiya, Y. Shimizu, K. Ohishi, and S. Utsumi. 1996. Endotoxin-induced enhancement of glucose influx into murine peritoneal macrophages via GLUT1. *Infect. Immun.* 64:108–112.

Gamelli, R.L., H. Liu, L.K. He, and C.A. Hofmann. 1996. Augmentations of glucose uptake and glucose transporter-1 in macrophages following thermal injury and sepsis in mice. *J. Leukoc. Biol.* 59:639–647.

Hansson, G.K., and M. Björkholm. 2010. Medicine. Tackling two diseases with HDL. *Science.* 328:1641–1642. http://dx.doi.org/10.1126/science.1191663

Hawkinson, J.E., M. Acosta-Burruel, and P.L. Wood. 1996. The metabotropic glutamate receptor antagonist L-2-amino-3-phosphonopropionic acid inhibits phosphoserine phosphatase. *Eur. J. Pharmacol.* 307:219–225. http://dx.doi.org/10.1016/0014-2999(96)00253-1

Herman, M.A., and B.B. Kahn. 2006. Glucose transport and sensing in the maintenance of glucose homeostasis and metabolic harmony. *J. Clin. Invest.* 116:1767–1775. http://dx.doi.org/10.1172/JCI29027

Jose, C., N. Bellance, and R. Rossignol. 2011. Choosing between glycolysis and oxidative phosphorylation: a tumor's dilemma? *Biochim. Biophys. Acta.* 1807:552–561. http://dx.doi.org/10.1016/j.bbabio.2010.10.012

Kelly, L.M., Q. Liu, J.L. Kutok, I.R. Williams, C.L. Boulton, and D.G. Gilliland. 2002. FLT3 internal tandem duplication mutations associated with human acute myeloid leukemias induce myeloproliferative disease in a murine bone marrow transplant model. *Blood.* 99:310–318. http://dx.doi.org/10.1182/blood.V99.1.310

Kumar, N.B., A. Kazi, T. Smith, T. Crocker, D. Yu, R.R. Reich, K. Reddy, S. Hastings, M. Exterman, L. Balducci, et al. 2010. Cancer cachexia: traditional therapies and novel molecular mechanism-based approaches to treatment. *Curr. Treat. Options Oncol.* 11:107–117. http://dx.doi.org/10.1007/s11864-010-0127-z

Lumeng, C.N., and A.R. Saltiel. 2011. Inflammatory links between obesity and metabolic disease. *J. Clin. Invest.* 121:2111–2117. http://dx.doi.org/10.1172/JCI57132

Lunt, S.Y., and M.G. Vander Heiden. 2011. Aerobic glycolysis: meeting the metabolic requirements of cell proliferation. *Annu. Rev. Cell Dev. Biol.* 27:441–464. http://dx.doi.org/10.1146/annurev-cellbio-092910-154237

Muoio, D.M., R.C. Noland, J.P. Kovalik, S.E. Seiler, M.N. Davies, K.L. DeBalsi, O.R. Ilkayeva, R.D. Stevens, I. Kheterpal, J. Zhang, et al. 2012. Muscle-specific deletion of carnitine acetyltransferase compromises glucose tolerance and metabolic flexibility. *Cell Metab.* 15:764–777. http://dx.doi.org/10.1016/j.cmet.2012.04.005

Odegaard, J.I., and A. Chawla. 2011. Alternative macrophage activation and metabolism. *Annu. Rev. Pathol.* 6:275–297. http://dx.doi.org/10.1146/annurev-pathol-011110-130138

Out, R., W. Jessup, W. Le Goff, M. Hoekstra, I.C. Gelissen, Y. Zhao, L. Kritharides, G. Chimini, J. Kuiper, M.J. Chapman, et al. 2008. Coexistence of foam cells and hypocholesterolemia in mice lacking the ABC transporters A1 and G1. *Circ. Res.* 102:113–120. http://dx.doi.org/10.1161/CIRCRESAHA.107.161711

Pikman, Y., B.H. Lee, T. Mercher, E. McDowell, B.L. Ebert, M. Gozo, A. Cuker, G. Wernig, S. Moore, I. Galinsky, et al. 2006. MPLW515L is a novel somatic activating mutation in myelofibrosis with myeloid metaplasia. *PLoS Med.* 3:e270. http://dx.doi.org/10.1371/journal.pmed.0030270

Rofe, A.M., C.S. Bourgeois, R. Bais, and R.A. Conyers. 1988. The effect of tumour-bearing on 2-deoxy[U-14C]glucose uptake in normal and neoplastic tissues in the rat. *Biochem. J.* 253:603–606.

Samudio, I., R. Harmancey, M. Fiegl, H. Kantarjian, M. Konopleva, B. Korchin, K. Kaluarachchi, W. Bornmann, S. Duvvuri, H. Taegtmeyer, and M. Andreeff. 2010. Pharmacologic inhibition of fatty acid oxidation sensitizes human leukemia cells to apoptosis induction. *J. Clin. Invest.* 120:142–156. http://dx.doi.org/10.1172/JCI38942

Vander Heiden, M.G., L.C. Cantley, and C.B. Thompson. 2009. Understanding the Warburg effect: the metabolic requirements of cell proliferation. *Science.* 324:1029–1033. http://dx.doi.org/10.1126/science.1160809

Wagers, A.J., R.I. Sherwood, J.L. Christensen, and I.L. Weissman. 2002. Little evidence for developmental plasticity of adult hematopoietic stem cells. *Science.* 297:2256–2259. http://dx.doi.org/10.1126/science.1074807

Westerterp, M., S. Gourion-Arsiquaud, A.J. Murphy, A. Shih, S. Cremers, R.L. Levine, A.R. Tall, and L. Yvan-Charvet. 2012. Regulation of hematopoietic stem and progenitor cell mobilization by cholesterol efflux pathways. *Cell Stem Cell.* 11:195–206. http://dx.doi.org/10.1016/j.stem.2012.04.024

Wood, T.E., S. Dalili, C.D. Simpson, R. Hurren, X. Mao, F.S. Saiz, M. Gronda, Y. Eberhard, M.D. Minden, P.J. Bilan, et al. 2008. A novel inhibitor of glucose uptake sensitizes cells to FAS-induced cell death. *Mol. Cancer Ther.* 7:3546–3555. http://dx.doi.org/10.1158/1535-7163.MCT-08-0569

Yuneva, M.O., T.W.M. Fan, T.D. Allen, R.M. Higashi, D.V. Ferraris, T. Tsukamoto, J.M. Matés, F.J. Alonso, C. Wang, Y. Seo, et al. 2012. The metabolic profile of tumors depends on both the responsible genetic lesion and tissue type. *Cell Metab.* 15:157–170. http://dx.doi.org/10.1016/j.cmet.2011.12.015

Yvan-Charvet, L., P. Even, M. Bloch-Faure, M. Guerre-Millo, N. Moustaid-Moussa, P. Ferre, and A. Quignard-Boulange. 2005. Deletion of the angiotensin type 2 receptor (AT2R) reduces adipose cell size and protects from diet-induced obesity and insulin resistance. *Diabetes.* 54:991–999. http://dx.doi.org/10.2337/diabetes.54.4.991

Yvan-Charvet, L., M. Ranalletta, N. Wang, S. Han, N. Terasaka, R. Li, C. Welch, and A.R. Tall. 2007. Combined deficiency of ABCA1 and ABCG1 promotes foam cell accumulation and accelerates atherosclerosis in mice. *J. Clin. Invest.* 117:3900–3908.

Yvan-Charvet, L., C. Welch, T.A. Pagler, M. Ranalletta, M. Lamkanfi, S. Han, M. Ishibashi, R. Li, N. Wang, and A.R. Tall. 2008. Increased inflammatory gene expression in ABC transporter-deficient macrophages: free cholesterol accumulation, increased signaling via toll-like receptors, and neutrophil infiltration of atherosclerotic lesions. *Circulation.* 118:1837–1847. http://dx.doi.org/10.1161/CIRCULATIONAHA.108.793869

Yvan-Charvet, L., T.A. Pagler, E.L. Gautier, S. Avagyan, R.L. Siry, S. Han, C.L. Welch, N. Wang, G.J. Randolph, H.W. Snoeck, and A.R. Tall. 2010. ATP-binding cassette transporters and HDL suppress hematopoietic stem cell proliferation. *Science.* 328:1689–1693. http://dx.doi.org/10.1126/science.1189731

Zou, C., Y. Wang, and Z. Shen. 2005. 2-NBDG as a fluorescent indicator for direct glucose uptake measurement. *J. Biochem. Biophys. Methods.* 64:207–215. http://dx.doi.org/10.1016/j.jbbm.2005.08.001